LAWRENCE
LIVERMORE
NATIONAL
LABORATORY

LLNL-TR-840790-DRAFT

IER-501 CED-3b: Experiment Execution Summary for the Pulsed-Neutron Die-¬Away Experimental Testbed for Thermal Scattering Law Benchmarks (PNDA)

D. Siefman, W. Zywiec, R. Araj, C. Percher, D. Heinrichs

October 4, 2022

Disclaimer

This work performed under the auspices of the U.S. Department of Energy by Lawrence Livermore National Laboratory under Contract DE-AC52-07NA27344.

IER-501 CED-3b: Experiment Execution Summary for the Pulsed-Neutron Die-Away Experimental Testbed for Thermal Scattering Law Benchmarks (PNDA)

Daniel Siefman, William Zywiec, Ruby Araj, Catherine Percher, and David Heinrichs

Lawrence Livermore National Laboratory
Nuclear Criticality Safety Division

9/30/2022

Lawrence Livermore National Laboratory, 7000 East Avenue, P.O. Box 808, L-198, Livermore, California, USA, 94551-0808

Auspices

This work performed under the auspices of the U.S. Department of Energy by Lawrence Livermore National Laboratory under Contract DE-AC52-07NA27344.

Acknowledgments

This work was supported by the United States Department of Energy (DOE) Nuclear Criticality Safety Program (NCSP), funded and managed by the National Nuclear Security Administration for the DOE.

0 Executive Summary

This report summarizes the experiments done for IER-501, a testbed for pulsed-neutron die-away (PNDA) experiments at Lawrence Livermore National Laboratory (LLNL). The PNDA experiments were conducted in two separate two-day campaigns: one campaign for high-density polyethylene and another for Lucite. All experiments were performed at Lawrence Livermore Laboratory. They will become high-quality benchmarks that serve to optimize and validate thermal neutron scattering laws (TSLs), which are high-priority nuclear data for the Department of Energy's Nuclear Criticality Safety Program (NCSP).

The report presents the PNDA design and its equipment, and it documents the experimental die-away curves. It presents the characterization measurements that have been performed to-date. Importantly, mass spectrometry measurements to determine sample impurities were not yet completed. These will be included in the final benchmark. The report gives the fitted decay constants for the die-away curves of each target sample. It also provides the data for the die-away curves in the appendices. The HDPE experiments examined twelve targets of varying size. The Lucite measurements included ten targets of varying size. Experimenters in the campaign were Daniel Siefman, William Zywiec, and Ruby Araj.

0.1 Table of Contents

1 Introduction

There is a strong need for new benchmarks to validate neutron thermal scattering laws (TSLs) [1]. Lawrence Livermore National Laboratory (LLNL) has designed a Pulsed-Neutron Die Away (PNDA) testbed for this purpose [2] [3] [4] [5]. The experiment has a deuterium-tritium (D-T) neutron generator that impinges a 10^{-5} to 10^{-3} s, mono-energetic pulse of 14.1 MeV neutrons on a target sample. After the pulse, the neutron population moderates and establishes a thermal equilibrium within the sample, with a fundamental spatial mode and characteristic decay-time eigenvalue. The eigenvalue can be extracted from the experimental measurements of the neutron flux coming off the surface of the sample and then used as an integral parameter to validate nuclear data involved with neutron migration, thermalization, and absorption. For certain materials and geometric configuration, the eigenvalue is heavily influenced by thermal neutron scattering of only the target material. For that reason, a PNDA experiment can have a higher sensitivity to TSLs than is commonly available with the k_{eff} parameter in critical experiments [6] [7].

After the neutron pulse, Eq. 1 describes the neutron population at thermal equilibrium and in the fundamental spatial mode. Here, **r** is a spatial location, *t* is time, *R(t)* is the background room return of neutrons, and α [s^{-1}] is the characteristic flux decay-time eigenvalue, or the integral parameter of the experiment.

$$\phi(\mathbf{r},t) = \phi_0(\mathbf{r})\exp(-\alpha t) + R(t) \qquad 1$$

The PNDA analysis requires calculating α, for both experimental and simulated data, by fitting the parameters of Eq. 1 to a neutron counts vs. time curve. Figure 1.1 shows a simulated pulsed die-away curve from MCNP6.2® [8]. At 0.66 ms the neutron-source pulse ends, and the neutrons diffuse through the target material and travel to the detector. When the pulse is turned off, the counts in the detector exhibit an exponentially decaying behavior after equilibrium is reached. An exponential fit with non-linear least squares is performed on the simulated neutron counts to determine α. The fit algorithm varies the parameters φ_0 and α to minimize the cost function, χ^2, between the MCNP6.2® tally and the exponential function.

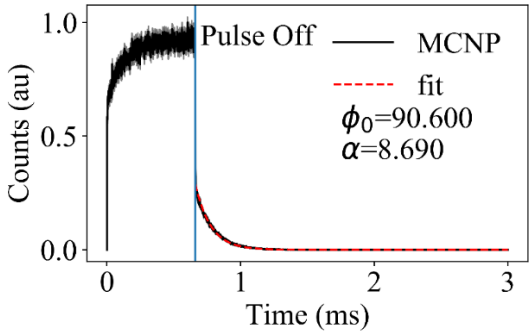

Figure 1.1: Example pulsed die away curve from a simulation of the PNDA testbed.

Eq. 2 describes α in further detail and shows how the experimental design can be manipulated to emphasize the physics of TSLs. D_0 [cm^2-s^{-1}] is the asymptotic diffusion coefficient[a] in an infinite medium of the target material, C [cm^4-s^{-1}] is the "cooling coefficient," B_0^2 [cm^{-2}] is the geometric buckling, *v* is the thermal neutron velocity (2.2 x 10^5 cm/s), and Σ_a [cm^{-1}] is the macroscopic absorption cross section. The cooling

[a] Some authors call D_0 the "diffusion coefficient" but using the term *asymptotic* helps to avoid confusion with the diffusion coefficient that has units of cm.

coefficient captures a geometric effect where more high-energy neutrons leak at the system boundaries, which causes the average neutron population to be at a temperature lower than thermodynamic equilibrium.

$$\alpha = \overline{\nu\Sigma_a} + B_0^2 D_0 - C B_0^4 \quad (2)$$

C is often very small relative to the absorption and diffusion terms and has a small impact on α. The exception to this is when the geometric buckling is very large, and the B_0^4 term becomes very important. In most cases, α is a nearly linear function of B_0^2 and the slope depends on the material cross sections.

For each target, B_0^2 can be changed by altering a certain geometric dimension, which would be done to manipulate how α is affected by different physics of the system. For instance, when the target sample is large and B_0^2 is small, α depends mostly on absorption (Σ_a), *i.e.* not on TSLs. When the target sample is small, B_0^2 is large and α depends primarily on D_0, which itself is highly influenced by the physics of thermal scattering. Fundamentally, the sensitivity of α to thermal scattering increases with B_0^2, or increases as the target sample size decreases.

2 Experiment Description

2.1 The PNDA Testbed

The PNDA testbed experiments are performed without the use of fissile material, requiring only the non-hazardous moderators of interest. As such, the PNDA benchmark experiments eliminate the need for special handling and may be executed at non-nuclear facilities. The PNDA experimental program utilizes existing LLNL resources, including low-scatter facilities, available neutron generators, well-characterized ^{3}He neutron detectors (with the additional ability to employ state-of-the-art scintillator detectors in later iterations), and on-hand, high-quality data acquisition systems capable of nanosecond time-resolution.

The experimental setup is shown by Figure 2.1. The testbed is comprised of a high-density, 5%-borated, polyethylene shielding box, lined with cadmium to mitigate the effects of room return. The moderating material is centered on a hole in the bottom of the shielding box. This target is easily switched out, allowing for fast turn-around of benchmark data for different materials. The neutron generator is placed underneath the target. Cylindrical ^{3}He neutron detectors are placed within the shielding box. The detector output is sent to the data acquisition system, via narrow cable feedthrough to minimize neutron streaming paths.

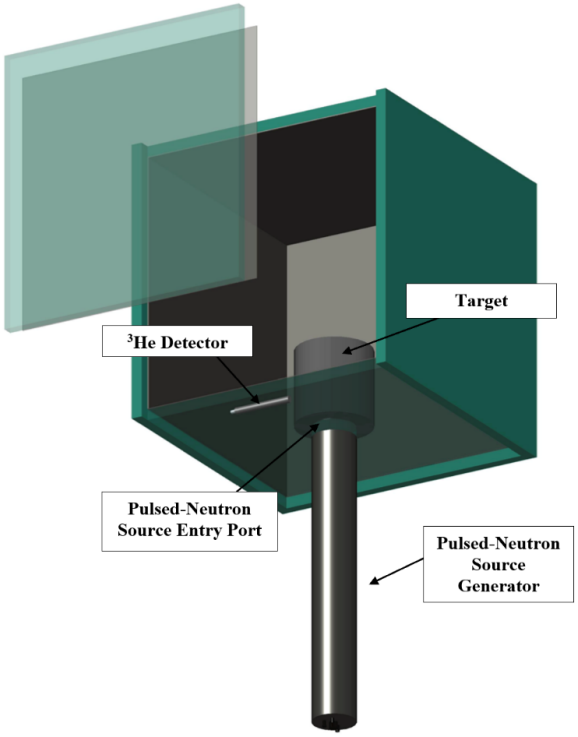

Figure 2.1: AutoCAD® rendering of the PNDA testbed (bottom view).

2.2 Low-Scatter Facilities

The experiments were conducted in Building 255, Room 183A at LLNL. As a heavily shielded facility, it allowed the generator to be operated at maximal settings to produce the largest neutron source term. Furthermore, it helped to reduce room-return background effects. Room 183A is relatively large, with high ceilings and a false floor made of aluminum grating, and is surrounded by concrete. The PNDA experiments were maintained at least 10 feet away from the walls and ceiling, and 6-10 feet away from the concrete floor, by mounting the shielding box on a table made of aluminum T-strut. The neutron generator was suspended below or perpendicular to the box, above the false floor. A high-fidelity MCNP® model of the facility (Figure 2.2), used for previous studies requiring low-scattering environments, will be integrated into final benchmark simulations (CED-4a/4b) of the PNDA experiments.

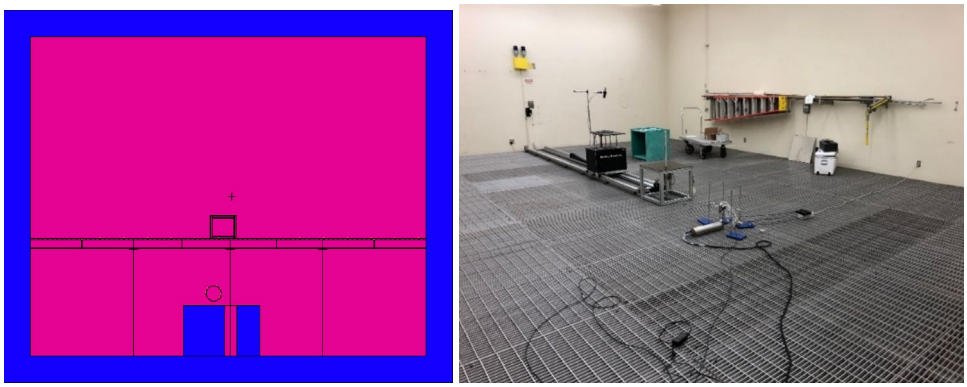

Figure 2.2: An MCNP® model of the B255 low scatter facility (left) and the facility itself (right).

2.3 Shielding Box

Sheets of 5%-borated high-density polyethylene (HDPE) (Shieldwerx™ 201HD) were procured to construct the outer shielding box walls. The borated HDPE serves as a neutron moderator and poison to eliminate room return from the facility walls and equipment. The interior of the box is lined with 1/8" thick cadmium sheets to further reduce room return. The neutron generator can be placed horizontal to the box or directly below a hole in the bottom of the box. The shielding box is easily disassembled, making it portable and reconfigurable to other geometries. For the final benchmark, detailed impurity analyses will be taken of the borated HDPE, along with dimensional measurements to determine and deviations from the requested dimensions given to the manufacturer. Figure 2.3 provides design dimensions of the shielding box and the cadmium liner. Figure 2.4 shows the shielding box in the experimental configuration. The neutron generator was located beneath box. The whole box rests upon a support structure.

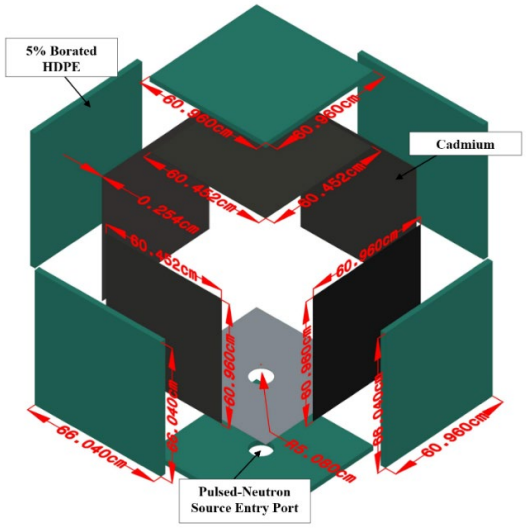

Figure 2.3: An AutoCAD® rendering of the shielding box (exploded view). The as built Shieldwerx™ borated HDPE box to be used in the PNDA experimental campaign.

Figure 2.4: Shielding box in the experimental configuration.

Table 2-1 lists the manufacturer-quoted 5%-borated HDPE composition. The last two rows of the table were not given in the manufacturer's specifications but were calculated using the given ratios of hydrogen

to boron in the datasheet and the typical relative weight-percentages of oxygen and carbon in HDPE. More detailed chemical analyses will be done for the final benchmark.

Table 2-1: SWX-201HD chemical composition data of the HDPE shielding box.

Composition Data	Weight %
Hydrogen	11.70%
$^{10}B/^{11}B$ isotope distribution	19.6%/80.4%
Boron	5%
Oxygen	22.40%
Carbon	61.73%

2.4 Moderating Targets

For the initial LLNL PNDA measurements, two materials were investigated: HDPE and Lucite. Both materials were procured from Curbell Plastics and cut to size by the machine shops at LLNL. Figure 2.5 shows the first eight HPDE cylinders. The sizes for each cylinder are presented in Table 2-4. As of the writing of this report, some of the inspections of the cylinders have been completed, including dimensional analyses and density measurements. The mass spectroscopy measurements were not yet completed.

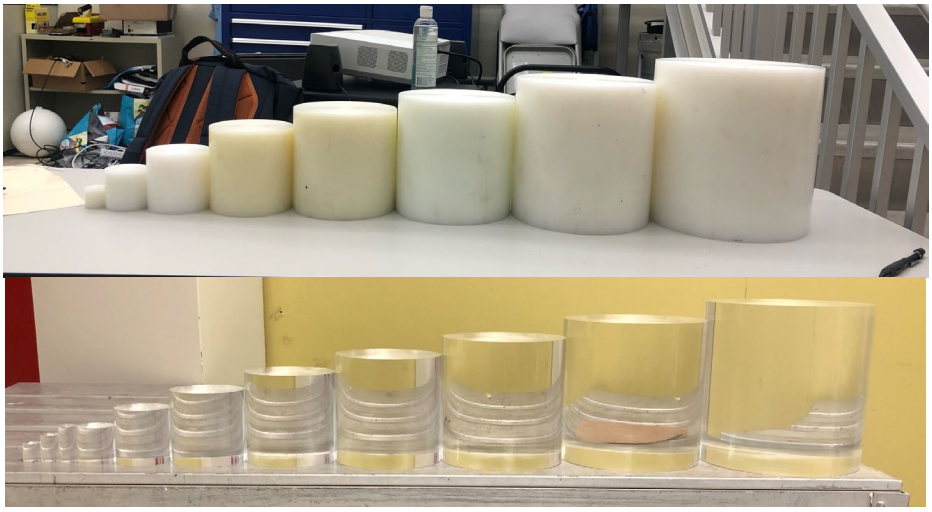

Figure 2.5: Some of the HDPE (top) and Lucite (bottom) cylinders.

Dimensional Inspection Laboratories (DIL) measured the dimensions of the moderating targets. DIL is an ISO/IEC 1025:2017 accredited facility (PFL Accreditation #66265). Their measurements were done with equipment that meets ANSI Y14.5-2009; ISO/IEC 17025:2017, and ISO 10012-1. They used a B241 MITUTOYO CMM (#8403262) whose accuracy is known to ± 0.000762 cm. The measurements were done at 21.1ºC and 40% humidity. The length, diameter, and roundness of the cylinders were all measured. The measurements were all done at three different points, with the average of the points to be used in benchmark models of the experiment. Roundness is the measure of how closely the shape of an object approaches that of a mathematically perfect circle. It is calculated with the maximum and minimum measured diameter, as in Eq. 3.

$$roundness = \frac{D_{max} - D_{min}}{2} \quad 3$$

Table 2-2 and Table 2-3 present the measured lengths of the HDPE and Lucite cylinders. The length was measured (Figure 2.6) at three locations on the cylinders' face: at the center, the left most edge, and the right most edge.

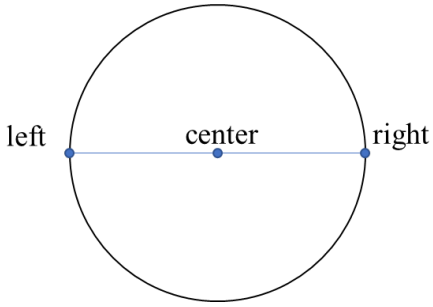

Figure 2.6: Measurement locations on the cylinder face.

Table 2-2: Measured lengths of the HDPE cylinders.

	Length (cm)				
ID:	Left	Center	Right	Mean	Std. Dev.
HDPE-1D-1H	2.55501	2.54495	2.55016	2.55004	0.00411
HDPE-2D-2H	5.09918	5.07589	5.09394	5.08967	0.00998
HDPE-3D-3H	7.65828	7.62648	7.65244	7.645733	0.01382
HDPE-4D-4H	10.82264	10.7774	10.8297	10.80989	0.02319
HDPE-5D-5H	13.45583	13.3807	13.461	13.43251	0.03672
HDPE-6D-6H	15.56652	15.4775	15.5535	15.53249	0.03925
HDPE-7D-7H	18.25965	18.2428	18.2444	18.24892	0.00761
HDPE-8D-8H	20.96064	20.9517	20.957	20.95646	0.00366
HDPE-9D-9H	22.92261	22.8518	22.9083	22.89426	0.03057
HDPE-10D-10H	25.40287	25.4036	25.4154	25.40731	0.00575
HDPE-11D-11H	27.98011	27.9639	27.9547	27.96626	0.01049

Table 2-3: Measured lengths of the Lucite cylinders. LUCITE-2D-2H is omitted as it was not measured at the time of writing this report.

	Length (cm)				
ID:	Left	Center	Right	Mean	Std. Dev.
LUCITE-1D-1H	2.54051	2.54152	2.54178	2.54127	0.00055
LUCITE-3D-3H	7.62533	7.62381	7.62406	7.62440	0.00067
LUCITE-4D-4H	10.16711	10.16533	10.16737	10.16660	0.00090
LUCITE-5D-5H	12.70559	12.70508	12.70635	12.70567	0.00052
LUCITE-6D-6H	15.24610	15.24610	15.24584	15.24601	0.00012
LUCITE-7D-7H	17.79397	17.79194	17.79168	17.79253	0.00102
LUCITE-8D-8H	20.32940	20.33016	20.32787	20.32914	0.00095
LUCITE-9D-9H	22.87143	22.86889	22.87270	22.87101	0.00158
LUCITE-10D-10H	25.40254	25.40279	25.40711	25.40415	0.00210

Table 2-4 and Table 2-5 provide the measured diameters and roundnesses of the HDPE cylinders. These were done at three different axial heights along the cylinder, with height given as from the bottom of the cylinder.

Table 2-4: Measured diameter of each HDPE cylinder. The diameter was evaluated at three different heights.

			Diameter (cm)	
Identification	Diameter (cm)	Measurement Height (cm)	Mean	Std. Dev.
HDPE-1D-1H	2.61379	0.51681	2.613483	0.00124
	2.61483	1.27620		
	2.61183	2.19037		
HDPE-2D-2H	5.24162	0.50795	5.242817	0.00233
	5.24607	2.28813		
	5.24076	4.57479		
HDPE-3D-3H	7.75147	0.63657	7.757133	0.00595
	7.76536	3.81097		
	7.75457	6.85922		
HDPE-4D-4H	10.75121	0.63276	10.7503	0.00913
	10.76101	5.71528		
	10.73869	10.1693		
HDPE-5D-5H	13.52763	1.25910	13.53452	0.01589
	13.55649	6.34390		
	13.51943	12.69601		
HDPE-6D-6H	15.59624	1.27302	15.61121	0.01648
	15.63416	8.25853		
	15.60322	13.96728		
HDPE-7D-7H	18.52102	1.27584	18.52972	0.00683
	18.53771	9.02183		
	18.53042	17.08175		
HDPE-8D-8H	21.23224	1.90569	21.23407	0.00599
	21.24215	10.16216		
	21.22782	19.94002		
HDPE-9D-9H	23.65611	1.52870	23.68864	0.02682
	23.72180	11.49264		
	23.68801	22.22576		
HDPE-10D-10H	25.99931	1.26522	25.99247	0.01459
	26.00592	12.61783		
	25.97219	24.38679		
HDPE-11D-11H	29.57297	1.26403	29.57784	0.00783
	29.57165	13.44872		
	29.58889	26.79649		

Table 2-5: Measured roundness of each HDPE cylinder. The roundness was evaluated at three different heights, with the being reported from the top of the cylinder as 0 cm.

			Roundness (-)	
Identification	Roundness (-)	Measurement Height (cm)	Mean	Std. Dev.
HDPE-1D-1H	0.00073	-0.51681	0.00082	0.00008
	0.00079	-1.27620		
	0.00093	-2.19037		
HDPE-2D-2H	0.01222	-0.50795	0.01134	0.00158
	0.01267	-2.28813		
	0.00912	-4.57479		
HDPE-3D-3H	0.00655	-0.63657	0.00622	0.00024
	0.00614	-3.81097		
	0.00598	-6.85922		
HDPE-4D-4H	0.05299	-0.63276	0.05400	0.00072
	0.05462	-5.71528		
	0.05439	-10.1693		
HDPE-5D-5H	0.05489	-1.25910	0.06134	0.00493
	0.06229	-6.34390		
	0.06685	-12.69601		
HDPE-6D-6H	0.02925	-1.27302	0.02929	0.00011
	0.02945	-8.25853		
	0.02918	-13.96728		
HDPE-7D-7H	0.00962	-1.27584	0.01215	0.00179
	0.01326	-9.02183		
	0.01357	-17.08175		
HDPE-8D-8H	0.01887	-1.90569	0.01817	0.00082
	0.01862	-10.16216		
	0.01701	-19.94002		
HDPE-9D-9H	0.02087	-1.52870	0.02350	0.00212
	0.02357	-11.49264		
	0.02606	-22.22576		
HDPE-10D-10H	0.01376	-1.26522	0.01107	0.00191
	0.01001	-12.61783		
	0.00945	-24.38679		
HDPE-11D-11H	0.00615	-1.26403	0.00563	0.00148
	0.00362	-13.44872		
	0.00712	-26.79649		

Table 2-6 and Table 2-7 provide the measured diameters and roundnesses of the Lucite cylinders. These were done at three different axial heights along the cylinder, with height given as from the bottom of the cylinder.

Table 2-6: Measured diameter of each Lucite cylinder. The diameter was evaluated at three different heights, with the being reported from the top of the cylinder as 0 cm. LUCITE-2D-2H is omitted as it was not measured at the time of writing this report.

			Diameter (cm)	
Identification	Diameter (cm)	Measurement Height (cm)	Mean	Std. Dev.
LUCITE-1D-1H	2.5464	0.381	2.5464	0.0002
	2.5461	1.270		
	2.5466	2.159		
LUCITE-3D-3H	7.6213	1.016	7.6267	0.0041
	7.6276	3.810		
	7.6312	6.604		
LUCITE-4D-4H	10.1697	1.016	10.1765	0.0049
	10.1788	5.080		
	10.1811	9.144		
LUCITE-5D-5H	12.6997	1.016	12.7057	0.0042
	12.7079	6.350		
	12.7094	11.684		
LUCITE-6D-6H	15.2494	1.016	15.2441	0.0059
	15.2471	7.620		
	15.2359	14.224		
LUCITE-7D-7H	17.8369	1.016	17.8373	0.0010
	17.8387	8.890		
	17.8364	16.764		
LUCITE-8D-8H	20.3738	1.016	20.3707	0.0030
	20.3716	10.160		
	20.3667	19.304		
LUCITE-9D-9H	22.9192	1.016	22.9171	0.0032
	22.9194	11.430		
	22.9179	21.844		
LUCITE-10D-10H	25.4615	1.016	25.4632	0.0028
	25.4671	12.700		
	25.4610	24.384		

Table 2-7: Measured roundness of each Lucite cylinder. The roundness was evaluated at three different heights, with the being reported from the top of the cylinder as 0 cm. LUCITE-2D-2H is omitted as it was not measured at the time of writing this report.

			Roundness (-)	
Identification	Roundness (-)	Measurement Height (cm)	Mean	Std. Dev.
LUCITE-1D-1H	0.001	0.381	0.0007	0.0002
	0.0007	1.270		
	0.0005	2.159		
LUCITE-3D-3H	0.0043	1.016	0.0048	0.0004
	0.0052	3.810		
	0.0050	6.604		
LUCITE-4D-4H	0.0005	1.016	0.0004	0.0000
	0.0004	5.080		
	0.0004	9.144		
LUCITE-5D-5H	0.0005	1.016	0.0007	0.0001
	0.0008	6.350		
	0.0008	11.684		
LUCITE-6D-6H	0.0006	1.016	0.0007	0.0001
	0.0007	7.620		
	0.0008	14.224		
LUCITE-7D-7H	0.0006	1.016	0.0006	0.0001
	0.0007	8.890		
	0.0005	16.764		
LUCITE-8D-8H	0.0007	1.016	0.0007	0.0001
	0.0005	10.160		
	0.0008	19.304		
LUCITE-9D-9H	0.0006	1.016	0.0007	0.0001
	0.0008	11.430		
	0.0008	21.844		
LUCITE-10D-10H	0.0004	1.016	0.0004	0.0001
	0.0005	12.700		
	0.0003	24.384		

Table 2-8 and Table 2-9 provide the measured densities of the HDPE and Lucite samples. Subsamples of the target materials were taken and provided to specialists at LLNL. They measured the density via the buoyancy method, by submerging the subsamples in a liquid and measuring the amount of liquid that was displaced. The Lucite samples, being denser than water, were measured via submersion in water. The HDPE samples were less dense than water and were submerged in isopropyl alcohol.

Table 2-8: Density measurements for the HDPE samples. Sample HDPE-11D-11H was not measured in time for this report. The density of the water was assumed to be 0.998 g/cm^3 for these measurements.

Sample	Dry mass (g)	Wet mass (g)	Displaced Water (g)	Displaced Water (cm^3)	Density (g/cm^3) Individual	Average	Standard Deviation
HDPE-1D-1H	0.594	0.101	0.493	0.624	0.952	0.951	0.001
	0.594	0.101	0.493	0.624	0.952		
	0.594	0.100	0.494	0.625	0.950		
HDPE-2D-2H	0.393	0.065	0.328	0.415	0.947	0.949	0.002
	0.392	0.066	0.326	0.413	0.950		
	0.391	0.066	0.325	0.411	0.950		
HDPE-3D-3H	0.926	0.154	0.772	0.977	0.948	0.948	0.001
	0.926	0.155	0.771	0.976	0.949		
	0.926	0.154	0.772	0.977	0.948		
HDPE-4D-4H	0.926	0.154	0.772	0.977	0.948	0.948	0.001
	0.926	0.155	0.771	0.976	0.949		
	0.926	0.154	0.772	0.977	0.948		
HDPE-5D-5H	0.635	0.103	0.532	0.673	0.943	0.943	0.000
	0.635	0.103	0.532	0.673	0.943		
	0.635	0.103	0.532	0.673	0.943		
HDPE-6D-6H	0.880	0.146	0.734	0.929	0.947	0.947	0.000
	0.880	0.146	0.734	0.929	0.947		
	0.880	0.146	0.734	0.929	0.947		
HDPE-7D-7H	0.875	0.142	0.733	0.928	0.943	0.943	0.000
	0.874	0.142	0.732	0.927	0.943		
	0.875	0.142	0.733	0.928	0.943		
HDPE-8D-8H	0.450	0.073	0.377	0.477	0.943	0.943	0.004
	0.451	0.075	0.376	0.476	0.948		
	0.448	0.071	0.377	0.477	0.939		
HDPE-9D-9H	0.419	0.068	0.351	0.444	0.943	0.943	0.000
	0.419	0.068	0.351	0.444	0.943		
	0.419	0.068	0.351	0.444	0.943		
HDPE-10D-10H	0.434	0.072	0.362	0.458	0.947	0.947	0.001
	0.432	0.071	0.361	0.457	0.945		
	0.432	0.072	0.360	0.456	0.948		

Table 2-9: Density measurements for the Lucite samples. Samples LUCITE-9D-9H and LUCITE-10D-10H were not measured in time for this report. The density of the isopropyl alcohol (IPA) was assumed to be 0.790 g/cm^3 for these measurements.

					Density (g/cm^3)		
Sample	Dry mass (g)	Wet mass (g)	Displaced IPA (g)	Displaced IPA (cm^3)	Individual	Average	Standard Deviation
LUCITE-1D-1H	1.024	0.162	0.862	0.864	1.186	1.184	0.0024
	1.017	0.157	0.860	0.862	1.180		
	1.020	0.161	0.859	0.861	1.185		
LUCITE-2D-2H	15.832	2.491	13.341	13.368	1.184	1.185	0.0002
	15.832	2.497	13.335	13.362	1.185		
	15.833	2.497	13.336	13.363	1.185		
LUCITE-3D-3H	2.064	0.330	1.734	1.737	1.188	1.186	0.0016
	2.061	0.324	1.737	1.740	1.184		
	2.061	0.326	1.735	1.738	1.186		
LUCITE-4D-4H	4.883	0.768	4.115	4.123	1.184	1.184	0.0000
	4.884	0.768	4.116	4.124	1.184		
	4.883	0.768	4.115	4.123	1.184		
LUCITE-5D-5H	2.165	0.337	1.828	1.832	1.182	1.182	0.0011
	2.165	0.336	1.829	1.833	1.181		
	2.165	0.340	1.825	1.829	1.184		
LUCITE-6D-6H	0.606	0.094	0.512	0.513	1.181	1.181	0.0000
	0.606	0.094	0.512	0.513	1.181		
	0.606	0.094	0.512	0.513	1.181		
LUCITE-7D-7H	0.189	0.036	0.153	0.153	1.233	1.218	0.0106
	0.189	0.033	0.156	0.156	1.209		
	0.187	0.033	0.154	0.154	1.212		
LUCITE-8D-8H	2.578	0.406	2.172	2.176	1.185	1.184	0.0003
	2.578	0.405	2.173	2.177	1.184		
	2.578	0.405	2.173	2.177	1.184		

2.5 Pulsed-Neutron Generator

A Thermo Scientific P 383 Neutron Generator (Figure 2.7) generates the neutrons that interrogate the target, which employs the D-T reaction. In comparison to a neutron generator employing a D-D reaction, the D-T reaction has an approximately 100 times larger neutron yield and creates ~14.1 MeV neutrons vs. ~2.5 MeV neutrons for D-D. The higher yield is important for PNDA experiments as it allows to improve the statistics of the neutron counts, thereby allowing for smaller samples with higher TSL sensitivity to be examined. While the tritium targets yield much higher neutron intensities, they have been found to produce a large background with a measured half-life of ~7.8 s, which is attributed to γ-rays from the reaction chain ^{16}O(n, p)^{16}N; $^{16}\text{N} \rightarrow {}^{16}\text{O} + \gamma + \beta^-$ (7.5 s) [13]. During current experimentation, no appreciable effects from γ-rays have been observed.

The P 383 model provides a high neutron yield without the necessity of active cooling, allowing it to be placed in a variety of orientations around and distances from the shielding box. Table 2-10 below lists some

of the P 383's technical specifications [1]. When operating at 90 kV and 50 μA, a neutron output of about 3×10^{8} n-s^{-1} is expected with an average neutron energy of 14.1 MeV.

The experiments in the low-scatter facility offer significantly more personnel shielding, which allowed the generator to be operated at its maximum conditions of 60 μA and 120 kV. Practically, this means that operations in the low-scatter facility offer a larger neutron source term, which along with reduced background, will provide better statistics in the pulsed die-away curves.

During operations, an error in the generator's software was discovered and reported to the manufacturer. The software did not accurately produce neutron pulses below 400 Hz. When set to frequencies below that threshold, it produced random frequencies that did not correspond to those requested. For example, a requested 150 Hz frequency was recorded to create a 620 Hz frequency. Additionally, these frequencies were never below 400 Hz, with low frequencies being required for large targets with longer die away times. Upon returning the generator to the manufacturer in September 2021, they updated the software and corrected the error. The generator can now operate down to 150 Hz.

Figure 2.7: The Thermo Scientific P 383 neutron generator.

Table 2-10: Thermo Scientific P 383 Specifications. The maximum and nominal yields per pulse were calculated with a maximum pulse width of 100 μs.

Parameter	Value
Nominal yield	3×10^{8} n-s^{-1}
Maximum yield	5×10^{8} n-s^{-1}
Nominal yield per pulse	3×10^{4} n
Maximum yield per pulse	5×10^{4} n
Voltage operating range	-40 kV to -130 kV
Pulse Range[a]	150 Hz to 20 kHz
Duty Cycle	5% - 100%
Minimum Pulse Width	5 μs
Pulse Rise/Fall Time	< 1.5/0.5 μs

2.6 Neutron Detectors and Electronics

Four LND, Inc. model 25177 cylindrical ^{3}He detectors (Table 2-11 and Figure 2.8) were procured and were used in the experimental campaign. The detectors were used in conjunction with electronics (combined

[a] The manufacturer's specifications give a minimum frequency of 250 Hz. Due to an error in the generator's software, it was sent back for repairs. During repair, it was requested for the software to be modified so that the minimum frequency would be decreased to 150 Hz, allowing pulse periods down to 6.66 ms.

high-voltage power supply, pre-amplifier, amplifier, and discriminator) from Precision Data Technology (model PDT20A-SHV-12V-C). The detectors were operated at 12 V and the pulse width is 50 ns.

Table 2-11: LND 25177 product specifications.

Maximum length (mm)	153.9
Maximum diameter (mm)	16
Effective length (mm)	23.88
Effective diameter (mm)	15.49
Operational Temperature Range °C	-40 to +80
Gas pressure (Torr)	3040
Effective volume (cm^3)	4.5

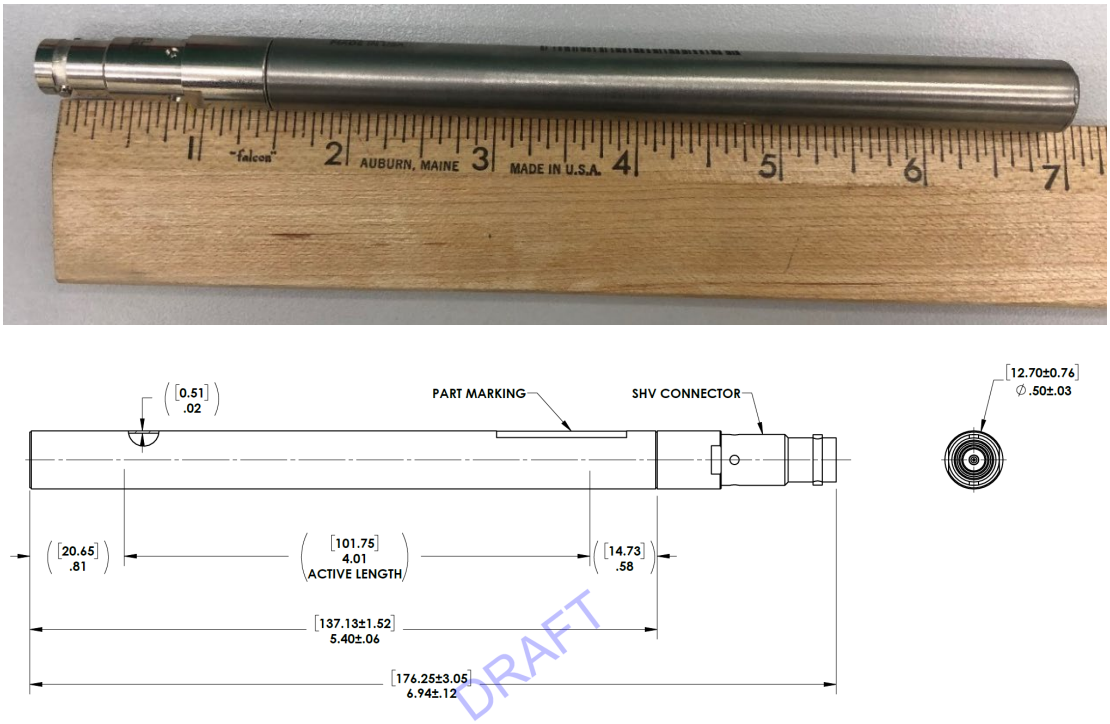

Figure 2.8: The LND 25177 ^{3}He neutron detector.

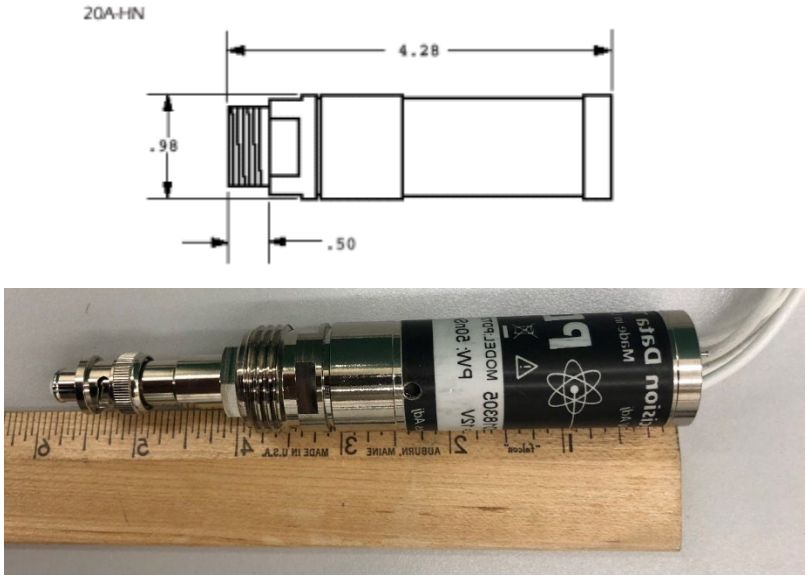

Figure 2.9 Precision data analyzer used as an integrated high-voltage power supply, pre-amplifier, amplifier, and pulse shaper. Dimensions are in inches.

Radiographic images were taken of the detectors to aid in modeling of the final benchmark. The non-destructive evaluation group at LLNL used the NSI X3000 is an X-ray imaging system to acquire computed tomographic data with a microfocus source and a flat panel. The measurements allow to determine the inner geometry of the detector and to better understand the composition of its components. Detailed modeling of the detectors will allow to determine if detector effects in the model are producing biases that may inappropriately attributed to the TSLs.

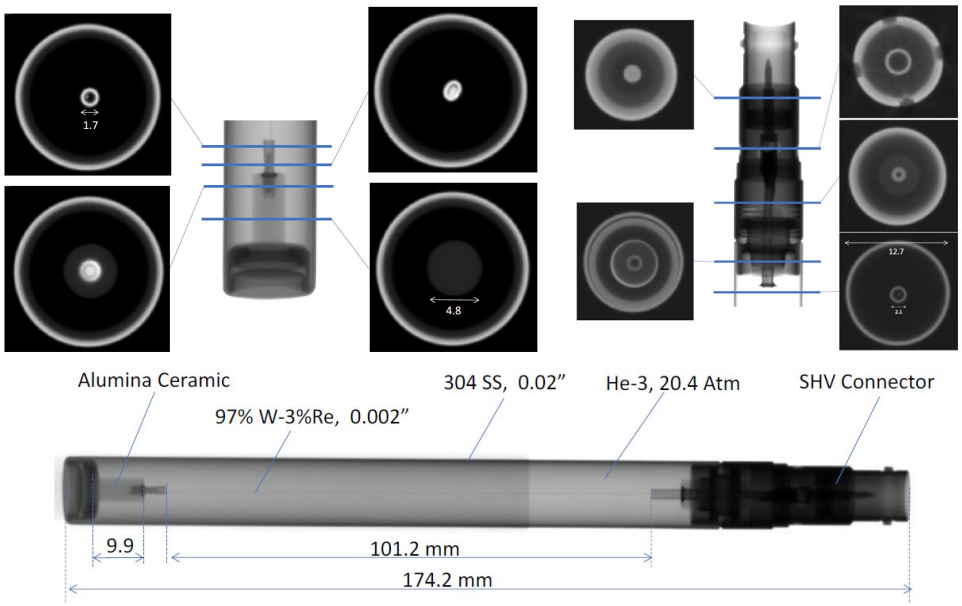

Figure 2.10: Computed tomography scans of the He-3 detectors that will be used to produce high-fidelity models for the final benchmark. Dimensions are in millimeters.

The neutron counts were registered with the Automated List Mode Module (ALMM) [14]. The ALMM was developed for use as a data acquisition system in safeguards applications, especially for neutron coincidence counting. It provides time tagged information with accuracy to 100 ns. For this experiment, the neutron detectors are connected to the ALMM's channel input along with the trigger output of the generator itself. Keeping track of the generator's pulses allows for the neutron counts of each detector to be summed together with correspondence to the time-tagged generator pulse that created them.

Figure 2.11 The ALMM data acquisition system used in the experimental setup. The four detectors are connected to channels 1-4 and the generator's source trigger is connected to channel 16.

3 Measurements

The measurements were conducted over several days in August and September 2022. For the measurements of all samples, the generator settings were modified to optimize the statistics of the data. Table 3-1 and Table 3-2 present the generator settings that were used for the HDPE and Lucite measurements, respectively. For smaller samples, the frequency was increased to allow for more pulses within the measurement window. The measurement time for these samples was also increased. This allowed for better statistics for these quickly decaying neutron populations.

Table 3-1: Generator setting for the HDPE measurements. For all measurements the current was set to 60 µA and the voltage was set to 120 kV.

ID:	Duration (min)	Frequency (Hz)	Period (ms)	Duty Factor (%)	Pulse Width (µs)
HDPE-1D-1H	90	2000	0.50	20.1	100.50
HDPE-2D-2H	60	1500	0.67	15.1	100.67
HDPE-3D-3H	30	1000	1.00	10.1	101.00
HDPE-4D-4H	30	667	1.50	6.7	100.45
HDPE-5D-5H	30	667	1.50	6.7	100.45
HDPE-6D-6H	30	570	1.75	5.7	100.00
HDPE-7D-7H	30	570	1.75	5.7	100.00
HDPE-8D-8H	30	500	2.00	5.1	102.00
HDPE-9D-9H	30	500	2.00	5.1	102.00
HDPE-10D-10H	30	450	2.22	4.51	100.22
HDPE-11D-11H	30	450	2.22	4.51	100.22

Table 3-2: Generator setting for the Lucite measurements. For all measurements the current was set to 60 µA and the voltage was set to 120 kV.

ID:	Duration (min)	Frequency (Hz)	Period (ms)	Duty Factor (%)	Pulse Width (µs)
LUCITE-1D-1H	60	750	1.33	7.6	101.33
LUCITE-2D-2H	60	667	1.50	6.7	100.45
LUCITE-3D-3H	45	500	2.00	5.1	102.00
LUCITE-4D-4H	40	450	2.22	4.6	102.22
LUCITE-5D-5H	35	400	2.50	4.1	102.50
LUCITE-6D-6H	30	400	2.50	4.1	102.50
LUCITE-7D-7H	30	400	2.50	4.1	102.50
LUCITE-8D-8H	30	300	3.33	3.1	103.33
LUCITE-9D-9H	30	300	3.33	3.1	103.33
LUCITE-10D-10H	30	300	3.33	3.1	103.33

At each measurement, the ambient temperature of the room was recorded with two independent measurements. These temperature readings may be used to account for any thermal expansion of the plastic targets and to use precise temperatures in the processing of the TSL data. The two devices were a Fluke 52 II thermometer and Model SH66A from Cooper Instrument Corporation, as shown in Figure 3.1. The temperature readings are given in Table 3-3 and Table 3-4.

Figure 3.1: Temperature reading devices used in the experiment.

Table 3-3: Temperature recordings during HDPE measurements.

	Temperature (°C)			
ID:	Fluke 52 II	Model SH66A	Average	Standard Deviation
HDPE-1D-1H	25.4	25.4	25.4	0.0
HDPE-2D-2H	26.0	25.8	25.9	0.1
HDPE-3D-3H	25.1	24.9	25.0	0.0
HDPE-4D-4H	25.3	25.2	25.3	0.0
HDPE-5D-5H	25.4	25.4	25.4	0.0
HDPE-6D-6H	25.6	25.8	25.7	0.1
HDPE-7D-7H	25.4	25.4	25.4	0.0
HDPE-8D-8H	25.8	25.8	25.8	0.0
HDPE-9D-9H	25.8	25.8	25.8	0.0
HDPE-10D-10H	24.9	24.9	24.9	0.0
HDPE-11D-11H	25.2	25.2	25.2	0.0

Table 3-4: Temperature recordings during Lucite measurements.

	Temperature (°C)			
ID:	Fluke 52 II	Model SH66A	Average	Standard Deviation
LUCITE-1D-1H	23.9	23.9	23.9	0.01
LUCITE-2D-2H	23.8	23.8	23.8	0.00
LUCITE-3D-3H	23.6	23.7	23.6	0.01
LUCITE-4D-4H	23.5	23.6	23.5	0.01
LUCITE-5D-5H	23.5	23.6	23.5	0.01
LUCITE-6D-6H	24.0	24.0	24.0	0.00
LUCITE-7D-7H	24.1	24.1	24.1	0.01
LUCITE-8D-8H	24.2	24.2	24.2	0.01
LUCITE-9D-9H	24.0	24.0	24.0	0.00
LUCITE-10D-10H	24.1	24.1	24.1	0.00

The experimental setup was placed in the low-scatter facility. The location of the box relative to the room walls was measured to the south-east corner of the box. Figure 3.2 shows the experimental setup in the low scatter room. Figure 3.3 and Figure 3.4 provide the measured distances to the shielding box during each set of measurements. This information will help to locate the box within the low-scatter room for the benchmark model. This information allows for analysis of the effect of room-return on the benchmark models.

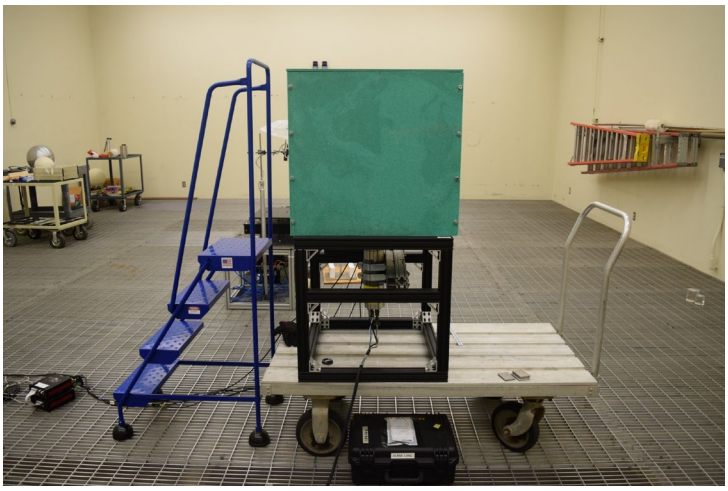

Figure 3.2: Experimental setup in the low scatter facility during the HDPE measurements.

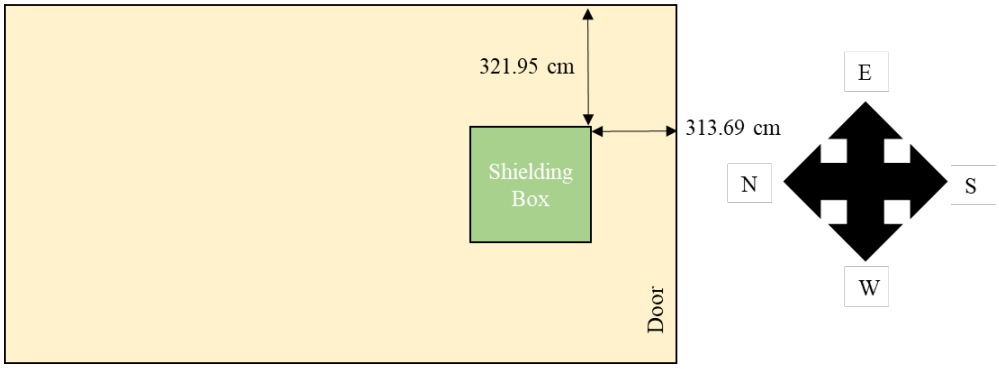

Figure 3.3: Placement of the shielding box relative to the room for the HDPE measurement.

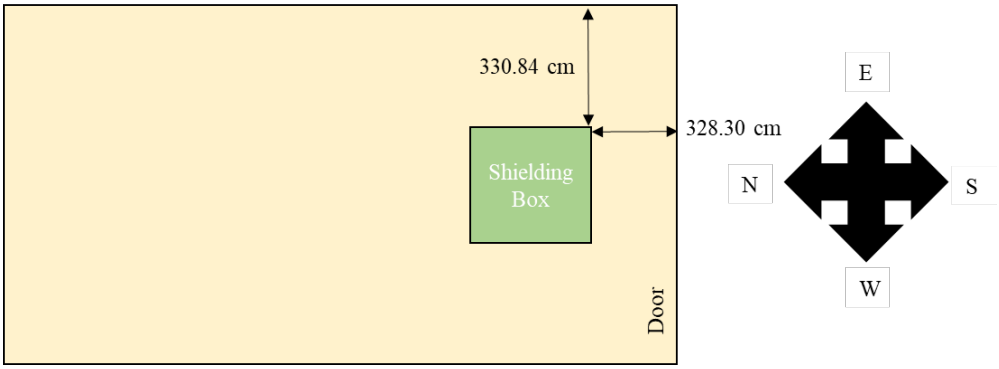

Figure 3.4: Placement of the shielding box relative to the room for the Lucite measurement.

The detectors were raised and lowered during the experiments so that their axial midpoint was at the axial midpoint of the target cylinders. In the cases where the detector was taller than the cylinder, the detector was lowered to its bottom most point, where the bottom face touched the detector holder. The height was determined by stacking aluminum shims that were 0.3175 cm thick. Knowing the location of the detectors will help in their modeling during the benchmark analysis. The detector holders were designed such that if the target sample was centered the box, the detectors would be centered at 90° intervals around the cylinder radius.

Table 3-5: Height of the detectors' bottom face from the top of the detector holder.

ID:	Detector Height from Top of Holder (cm)
HDPE/LUCITE-1D-1H	0
HDPE/LUCITE-2D-2H	0
HDPE/LUCITE-3D-3H	0
HDPE/LUCITE-4D-4H	0
HDPE/LUCITE-5D-5H	0
HDPE/LUCITE-6D-6H	1.27
HDPE/LUCITE-7D-7H	2.54
HDPE/LUCITE-8D-8H	3.81
HDPE/LUCITE-9D-9H	5.08
HDPE/LUCITE-10D-10H	6.35
HDPE-11D-11-H	7.62

Figure 3.5 and Figure 3.6 present the arrangement of the detectors around the targets during the measurements. Importantly, it details which detector was connected to which channel in the ALMM time-tagging electronics. Recording this information will help diagnose any possible issues with a single detector in the measurement.

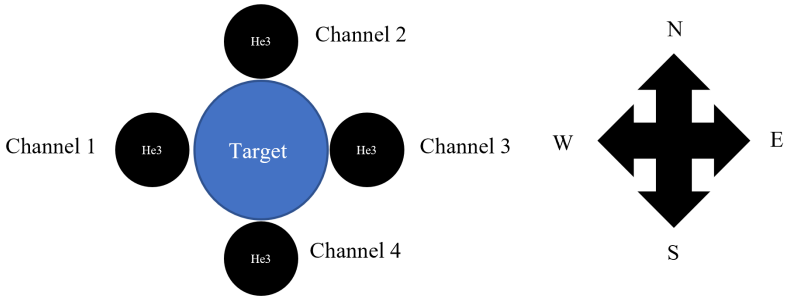

Figure 3.5: Arrangement of the detectors relative to their channel in the electronics during the HDPE measurement.

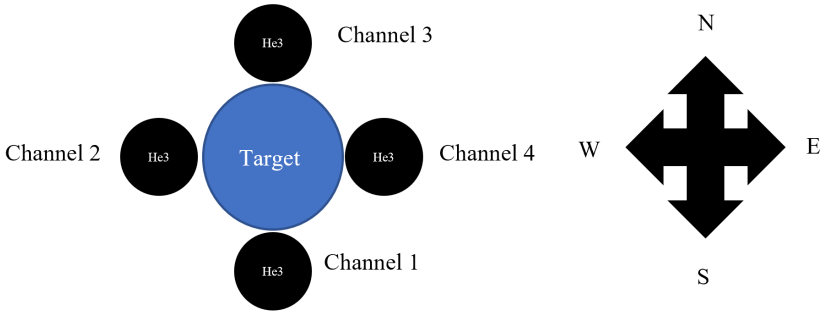

Figure 3.6: Arrangement of the detectors relative to their channel in the electronics during the Lucite measurement.

The target samples were centered in the shielding via two rulers attached to the detector holders. The samples were aligned so that they were centered in the box. Figure 3.7 and Figure 3.8 show the detector holders and the rulers, with Figure 3.8 specifically showing how a target sample would be aligned with the rulers. The experimenters believe that this alignment was accurate to within 1/16”, or 0.15875 cm.

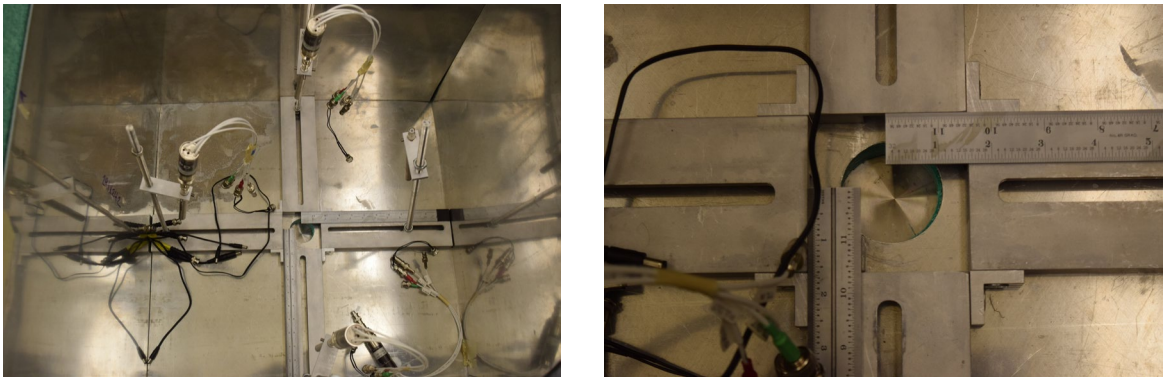

Figure 3.7: Detector holders and rulers used for alignment.

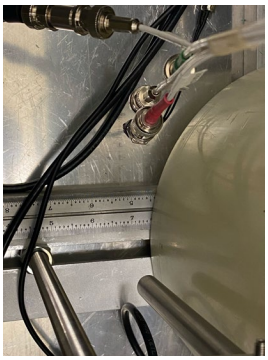

Figure 3.8: Example alignment of the HDPE-7D-7H sample.

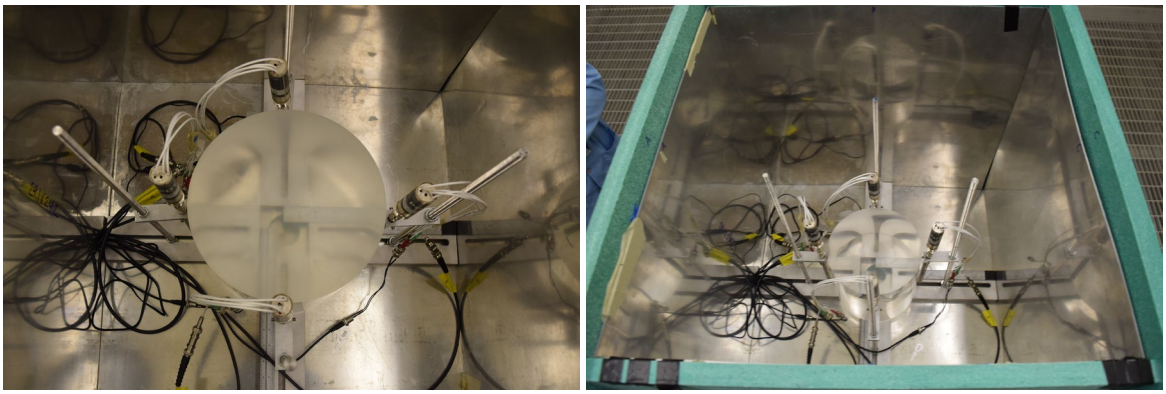

Figure 3.9: Measurement of a Lucite target.

Table 3-6 and Table 3-7 present the fitted decay constants from the HDPE and Lucite measurements, respectively. Additionally, they provide information about the fitting parameters used to extract the decay constants. The time-tagged data that correspond to the neutron counts and generator triggers were post-processed to create a single die-away curve. The neutron counts were summed into 1 μs bins for all cases.

The PNDA analysis requires calculating the decay constant, for either experimental or simulated data. The "wait time" method is the most commonly employed for this analysis. First the neutron counts as a function of time is measured. Next, an exponential is fit to these data to estimate the decay constant of the system after the pulse of neutrons. The fit must only be done after a sufficient amount of wait time so that only the neutron flux in the fundamental mode is used. Otherwise, the higher order modes will not have sufficiently

decayed away to provide a well-estimated and reproducible decay constant. The sufficient amount of time to wait depends on each sample size, as the magnitude of the buckling will determine the rate at which higher order modes decay away.

Each die-away curve needs a specific time interval for its fit, or else the decay constant may be over- or under-estimated. It is possible to over-estimate the decay constant by incorporating data from too early times, *i.e*. before either the flux is either fully thermalized or is in its fundamental spatial mode. It is also possible to underestimate or have excessively noisy decay constants by including data that are too late in the curve where room return is significant.

Our fitting approach is based on the previously described behavior: including too early time bins create overestimated decay constants and including too late time bins create underestimated or noisy decay constants. Importantly, when using data in the fundamental mode, the decay constants are consistent (within fitting uncertainty) despite varying time intervals. For the nominal data set (no perturbations to any nuclear data) we chose, for each target size, the data region where plateaued decay constants occurred. Table 3-6 and Table 3-7 present the start and stop regions that define the plateau over which the decay constant was averaged.

Table 3-6: Fitting parameters and fitted decay constants for the HDPE measurements.

	Time (ms)			α (1/ms)	
ID:	Interval	Start	Stop	Mean	Std. Dev.
HDPE-1D-1H	0.035	0.100	0.110	75.509	0.409
HDPE-2D-2H	0.040	0.170	0.190	29.273	0.248
HDPE-3D-3H	0.100	0.200	0.250	17.887	0.035
HDPE-4D-4H	0.100	0.300	0.400	12.484	0.033
HDPE-5D-5H	0.150	0.475	0.575	10.187	0.047
HDPE-6D-6H	0.175	0.560	0.660	9.133	0.028
HDPE-7D-7H	0.190	0.560	0.660	8.333	0.015
HDPE-8D-8H	0.250	0.560	0.660	7.791	0.010
HDPE-9D-9H	0.200	0.560	0.660	7.532	0.018
HDPE-10D-10H	0.200	0.560	0.660	7.252	0.013
HDPE-11D-11H	0.350	0.700	0.800	6.946	0.005

Table 3-7: Fitting parameters and fitted decay constants for the Lucite measurements.

	Time (ms)			α (1/ms)	
ID:	Interval	Start	Stop	Mean	Std. Dev.
LUCITE-1D-1H	0.100	0.115	0.125	76.773	0.238
LUCITE-2D-2H	0.100	0.165	0.175	33.911	0.180
LUCITE-3D-3H	0.100	0.130	0.160	20.051	0.050
LUCITE-4D-4H	0.300	0.185	0.285	13.804	0.010
LUCITE-5D-5H	0.300	0.335	0.435	10.611	0.009
LUCITE-6D-6H	0.300	0.500	0.600	8.821	0.010
LUCITE-7D-7H	0.300	0.510	0.610	7.653	0.008
LUCITE-8D-8H	0.300	0.510	0.610	6.884	0.009
LUCITE-9D-9H	0.300	0.535	0.635	6.365	0.008
LUCITE-10D-10H	0.300	0.760	0.860	5.896	0.006

Figure 3.10 and Figure 3.11 present the die-away curves for the two sets of moderators. For the final benchmark, the data will be given in two forms. The first is the raw, time-tags associated with the neutron detectors and the generator trigger. These files are very large and range from 10-20 GB in size. They will be uploaded with the final benchmark document. Their file names are given in Table 3-7.

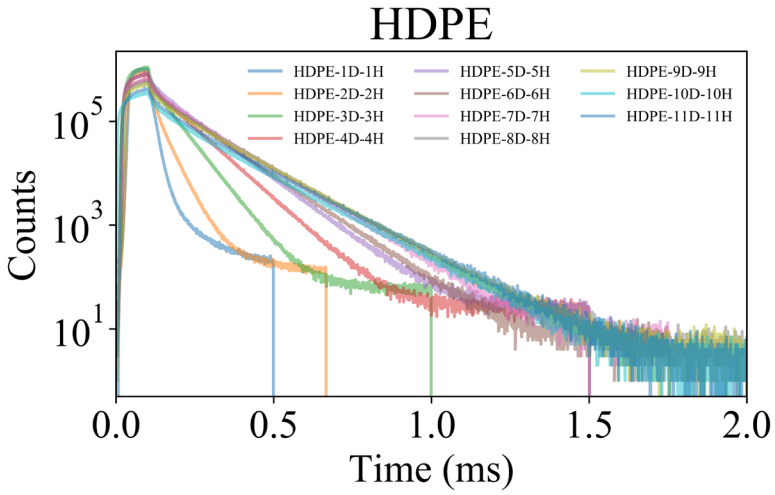

Figure 3.10: Die-away curves from the HDPE measurement.

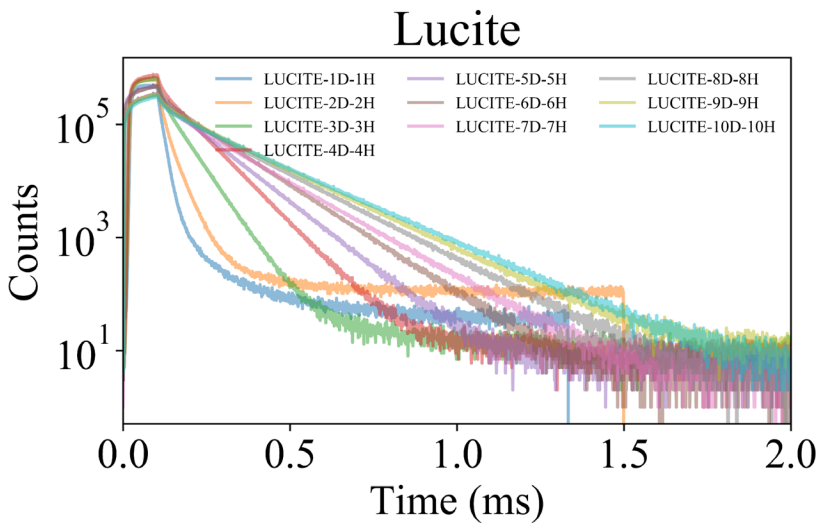

Figure 3.11: Die-away curves from the Lucite measurement.

Table 3-8: File names that contain the time-tagged data from the measurements.

ID:	File Name	ID:	File Name
LUCITE-1D-1H	LUCITE-1D-1H.txt	HDPE-1D-1H	HDPE-1D-1H.txt
LUCITE-2D-2H	LUCITE-2D-2H.txt	HDPE-2D-2H	HDPE-2D-2H.txt
LUCITE-3D-3H	LUCITE-3D-3H.txt	HDPE-3D-3H	HDPE-3D-3H.txt
LUCITE-4D-4H	LUCITE-4D-4H.txt	HDPE-4D-4H	HDPE-4D-4H.txt
LUCITE-5D-5H	LUCITE-5D-5H.txt	HDPE-5D-5H	HDPE-5D-5H.txt
LUCITE-6D-6H	LUCITE-6D-6H.txt	HDPE-6D-6H	HDPE-6D-6H.txt
LUCITE-7D-7H	LUCITE-7D-7H.txt	HDPE-7D-7H	HDPE-7D-7H.txt
LUCITE-8D-8H	LUCITE-8D-8H.txt	HDPE-8D-8H	HDPE-8D-8H.txt
LUCITE-9D-9H	LUCITE-9D-9H.txt	HDPE-9D-9H	HDPE-9D-9H.txt
LUCITE-10D-10H	LUCITE-10D-10H.txt	HDPE-10D-10H	HDPE-10D-10H.txt
		HDPE-11D-11H	HDPE-11D-11H.txt

4 Conclusions

IER-501 has completed the CED-3b stage of the integral experiment process for two target materials. The measurements have been completed and are documented in this report. The data presented here will form the basis for the benchmark evaluation that will be conducted in fiscal year 2023. The measurements investigated two moderating materials: high-density polyethylene and Lucite. Characterization of the moderating targets has progressed, but mass spectrometry measurements of their composition still need to be completed in order to develop high detail benchmark models.

5 References

[1] J. Holmes, M. Zerkle and D. Heinrichs, "Benchmarking a first-principles thermal neutron scattering law for water ice with a diffusion experiment," *EPJ Web of Conferences,* vol. 146, p. 13004, 2017.

[2] D. Siefman, E. Heckmaier, W. Zywiec and D. Heinrichs, "IER-501 CED-1: Preliminary Design of a New Pulsed-Neutron Die-Away Experimental Testbed for Thermal Scattering Law Benchmarks (PNDA)," Lawrence Livermore National Lab (LLNL), Livermore, CA, 2021.

[3] D. Siefman, C. K. A. Percher and D. Heinrichs, "IER-519 CED-2: Final Design for Thermal/Epithermal eXperiments (TEX) with Absorbers to Provide Validation Benchmarks for Hanford Tank Farms," Lawrence Livermore National Laboratory (LLNL-TR-817877), Livermore, CA, 2020.

[4] D. Siefman, W. Zywiec, C. Percher and D. Heinrichs, "New Pulsed Neutron Die Away Experiments in Light Water," in *American Nuclear Society Annual Conference (Criticality Safety Topical)*, Anaheim, 2022.

[5] D. Siefman, S. Coleman, J. Northrop, W. Zywiec, J. Holmes, M. Zerkle, D. Heinrichs and C. Percher, "Pulsed-Neutron Die-Away Experiments for Plastics and Neutron Thermal Scattering Laws," in *15th International Conference on Nuclear Data for Science and Technology*, Sacramento, 2022.

[6] D. Siefman, C. Percher and D. Heinrichs, "Sensitivity Analysis of H2O Pulsed-Neutron Die-Away Experiments to the H-H2O Thermal Scattering Law," in *Transactions of American Nuclear Society*, 2021.

[7] D. Siefman, M. Hursin, C. Percher and D. Heinrichs, "Uncertainty Quantification of a Light Water Pulsed-Neutron Die-Away Experiment to Thermal Neutron Scattering Laws," *Nuclear Science and Engineering,* pp. 1-11, 2022.

[8] MCNP6 User's Manual, Version 1.0, LA-CP-13-00614, Los Alamos National Laboratory, 2013.

[9] A. Bracci and C. Coceva, "The Diffusion Parameters of Thermal Neutrons in Water," *Il Nuovo Cimento,* vol. 4, pp. 59-66, 1956.

[10] G. von Dardel and N. G. Sjostrand, "Diffusion Parameters of Thermal Neutrons in Water," *Physical Review,* vol. 96, no. 5, pp. 1245-1249, 1954.

[11] J. Dorning, "Extrapolation Distances and Diffusion Parameters via Pulsed-Neutron Analysis," *Nuclear Science and Engineering ,* vol. 41, pp. 22-28, 1970.

[12] J. Manley, H. L.J. and E. Luebke, "The Mean Life of Neutrons in Water and the Hydrogen Capture Cross SEction," *Physical Review,* vol. 61, pp. 152-155, 1942.

[13] E. G. Silver, "A Pulsed-Neutron Investigation of the Effect of Temperature on the Decay of a Therman-Neutron in H20 Ice," *Nuclear Science an Engineering,* vol. 34, pp. 275-284, 1968.

[14] M. R. Newell, "New Developments in Safeguards Electronics," Los Alamos National Laboratory, LA-UR-17-29472, Los Alamos, NM, 2017.

[15] International Handbook of Evaluated Criticality Safety Benchmark Experiments, September 2016 Edition, NEA/NSC/DOC(95)03, Nuclear Energy Agency, Organisation for Economic Cooperation and Development, 2016.

[16] C. J. Wharton, E. H. Seabury, D. L. Chichester, A. J. Caffrey, J. Simpson and M. Lemchak, "X-Ray Measurements Of A Thermo Scientific P385 DD Neutron Generator," in *AIP Conference Proceedings*, 2011.

[17] J. Holmes, M. Zerkle and A. Hawari, "Validation of Themral Scattering Laws for Light Water at Elevated Temperatures with Diffusion Experiments," in *PHYSOR 2020: Transition to a Scalable Nuclear Future*, Cambridge, United Kingdom, 2020.

[18] S. Nassar and G. Murphy, "Pulsed-Neutron Diffusion Parameters in Spherical Water Systems," *Nuclear Science and Engineering,* vol. 35, pp. 70-79, 1969.